Control Barrier Function Based Visual Servoing for Underwater Vehicle Manipulator Systems under Operational Constraints

Shahab Heshmati-Alamdari, George C. Karras, Maryam Sharifi, George K. Fourlas

***Abstract*— This paper presents a novel control strategy for image-based visual servoing (IBVS) of underwater vehicle manipulator systems (UVMS) using control barrier functions (CBFs) to handle field of view (FoV) constraints and system's operational limitations such as manipulator joint limits and vehicle velocity performances. The proposed approach combines the advantages of IBVS, which provides visual feedback for control, with CBFs, which can formally enforce visibility and safety constraints on the UVMS's motion. A CBF-based control law is derived and integrated with the IBVS algorithm, which guarantees the satisfaction of FoV and system's operational constraints and ensure stability of the closed-loop system. To deal with FoV constraints, the proposed method uses a FoV index to estimate the degree of visibility of the scene, which is used to adjust the control inputs accordingly. The effectiveness of the proposed strategy is demonstrated through realistic simulation results, showing improved performance and safety of the UVMS under FoV and operational constraints compared to traditional IBVS methods. The results indicate that the proposed approach can handle the challenging underwater environment, UVMS dynamics and the operational constraints effectively, making it a valuable control strategy for practical applications of UVMS.**

I. Introduction

Unmanned Underwater Vehicles (UUVs) have become prevalent in various fields like marine science and offshore maintenance over the past decades [1]. These applications often require intervention abilities [2], driving increased attention towards Underwater Vehicle Manipulator Systems (UVMS) [3], a subset of Floating Base Mobile Manipulator System (FBMMS) [4]. Underwater interventions are typically conducted using Remotely Operated Vehicles (ROVs), equipped with manipulators for object manipulation, and controlled by human operators through a master-slave teleoperation setup [5], [6]. Recognizing human-robot teleoperation limitations, the scientific community is prioritizing the development of autonomous control systems for UVMS. Regardless of their intended use, UVMSs often require visual information to be integrated into their control scheme for effective autonomous grasping and manipulation in interaction tasks [7], [8]. This leads to the development of Visual Servoing, where the camera captures the environment and by employing proper vision algorithms [9] the visual feedback is utilized to determine the robot's control inputs.

Shahab Heshmati-alamdari is with the Section of Automation & Control, Department of Electronic Systems, Aalborg University, Denmark, Email: {shhe@se.aau.dk}. Maryam Sharifi is with ABB Corporate Research, Västerås, Sweden, Email: {maryam.sharifi@se.abb.com}. George C. Karras and George K. Fourlas are with the University of Thessaly, Department of Informatics and Telecommunications, Lamia, Greece Email: {gkarras,gfourlas@uth.gr}.

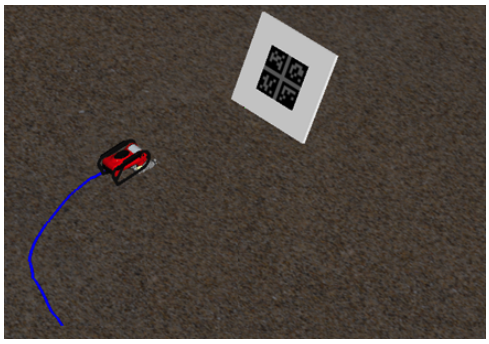

Fig. 1. The proposed CBF-IBVS scheme applied to a UVMS.

In terms of structure, Visual Servoing can be separated into three categories: (i) Position-Based Visual Servoing (PBVS), where visual features are used to calculate the 3D pose of the target and the control error is defined in Cartesian space, (ii) Image-Based Visual Servoing (IBVS), where the control error is directly calculated in the image plane, and (iii) 2-1/2 Visual Servoing, which combines the 3D PBVS with the 2D IBVS [10], [11].

In this work, we will use an IBVS scheme, recognized for superior local stability and robustness against camera inaccuracies and depth estimation errors, for mobile manipulation tasks [12]. One important challenge in visual servo control is the proper management of visibility constraints, ensuring that the image features stay within the camera's Field of View (FoV) during the robot's movement [13]. Apart from the visibility constraints, applying IBVS for UVMS poses challenges in ensuring safe, stable motion within operational constraints like joint limits and system kinematic singularities [14]. FoV limitation can restrict UVMS movement, putting the system at risk of unexpected behavior, damage or mission failure if operational constraints such as joint limits and kinematic singularities are not taken into account. Therefore, the challenge of implementing IBVS-UVMS control is heightened by various operational limitations such as visibility constraints, manipulator joint limits, and manipulability of the system, as well as modeling uncertainties in the vehicle-manipulator dynamics and camera calibration parameters.

Control Barrier Functions (CBFs) offer a potential solution to UVMS control challenges [15]. It provides a rigorous framework for control systems, ensuring safety and performance by keeping system behavior within desired constraints. CBFs offer a systematic and efficient way to confirm system behavior won't violate safety constraints, despite uncertainty and disturbances. This method has gained popularity in recent years in the fields of robotics and autonomous systems [16], and has been applied to various

domains, including aerial [17] ground [18] and underwater [19] vehicles, multi-agent systems [20], and safety-critical systems [21].

In this work, a novel IBVS control approach for underwater vehicle manipulator systems is proposed by integrating control barrier functions. The integration effectively addresses the operational limitations and visibility constraints of IBVS, as well as the uncertainties in the system dynamics, by utilizing control barrier functions to enforce safety constraints while achieving the desired IBVS objectives. This enables the system to accomplish its desired IBVS task with guaranteed visibility constraints while ensuring that the manipulator remains within its joint limits and the system operates within specified performance criteria (e.g., increased system manipulability). The control methodology is two-tiered, with each level regulated by suitable barrier functions: the first stage involves a CBF-IBVS controller for the UVMS camera frame, maintaining field of view constraints, and the second uses a CBF velocity controller for overall UVMS, tracking CBF-IBVS commands while respecting velocity limits. This strategy improves response characteristics, robustness to disturbances and modeling uncertainties, and has low computational complexity, making it suitable for real-time embedded systems. Its efficacy is demonstrated in extensive simulations, showing improved performance, safety, and robustness compared to traditional IBVS methods. To the authors' knowledge, no similar CBF-IBVS scheme for UVMSs previously reported in the related literature.

II. PROBLEM FORMULATION

This section first presents the kinematic and dynamic equations of the Underwater Vehicle Manipulator System, followed by standard IBVS modeling and FoV constraints definition.

A. Underwater Vehicle Manipulator System Modeling

Consider a n DoF UVMS comprised of a n_v actuated DoF underwater vehicle and a n_m DoF manipulator, resulting in a total of $n = n_v + n_m$. The state variables of the UVMS, represented as $\boldsymbol{q} = [\boldsymbol{q}_v^\top,\ \boldsymbol{q}_m^\top]^\top \in \Re^n$, include the vector $\boldsymbol{q}_v = [\boldsymbol{\eta}_1^\top, \boldsymbol{\eta}_2^\top]^\top \in \Re^6$ that describes the vehicle's position, represented by $\boldsymbol{\eta}_1 = [x_v, y_v, z_v]^\top$, and orientation, represented by the Euler angles $\boldsymbol{\eta}_2 = [\phi_v, \theta_v, \psi_v]^\top$, with respect to an inertial frame I. The vector $\boldsymbol{q}_m \in \Re^{n-6}$ represents the manipulator's joint angles. Consider also that the frame $\{E\}$ is attached to the end-effector of the UVMS and is described by a position vector $\boldsymbol{x}_e = [x_e, y_e, z_e]^\top \in \Re^3$ and a rotation matrix $\boldsymbol{R}_e = [\boldsymbol{n}_e, \boldsymbol{o}_e, \boldsymbol{\alpha}_e]$ relative to $\{I\}$. The rotational velocity of the end-effector, represented as $\boldsymbol{\omega}_e$, satisfies $\boldsymbol{S}(\boldsymbol{\omega}_e) = \dot{\boldsymbol{R}}_e\boldsymbol{R}_e^\top$, where $\boldsymbol{S}(\boldsymbol{\omega}_e)$ is the skew-symmetric matrix of $\boldsymbol{\omega}_e$. The linear velocity $\boldsymbol{t}_e$ and angular velocity $\boldsymbol{\omega}_e$ of the end-effector are combined into the vector $\boldsymbol{v}_e = [\boldsymbol{t}_e^\top, \boldsymbol{\omega}_e^\top]^\top \in \Re^6$. Without loss of generality, we have [22]:

$$\boldsymbol{v}_e = \boldsymbol{J}(\boldsymbol{q})\boldsymbol{\zeta} \tag{1}$$

where $\boldsymbol{\zeta} = [\boldsymbol{v}^\top, \dot{\boldsymbol{q}}_{m,i}^\top]^\top \in \Re^n$ includes the vehicle body and manipulator joint velocities $\boldsymbol{v}$, $\dot{\boldsymbol{q}}_{m,i},\ i \in \{1, \ldots, n-6\}$ respectively and $\boldsymbol{J}(\boldsymbol{q}) \in \Re^{6\times n}$ is the Jacobian matrix of the overall system [22]. Moreover, the UVMS dynamics can be written in general form, as [22]:

$$\boldsymbol{M}(\boldsymbol{q})\dot{\boldsymbol{\zeta}} + \boldsymbol{C}(\boldsymbol{q},\boldsymbol{\zeta})\boldsymbol{\zeta} + \boldsymbol{D}(\boldsymbol{q},\boldsymbol{\zeta})\boldsymbol{\zeta} + \boldsymbol{g}(\boldsymbol{q}) + \boldsymbol{\delta}(\boldsymbol{q},\boldsymbol{\zeta},t) = \boldsymbol{\tau} \tag{2}$$

where $\boldsymbol{\delta}(\boldsymbol{q},\boldsymbol{\zeta},t)$ encapsulates bounded unmodeled terms and external disturbances. Moreover, $\boldsymbol{\tau} \in \Re^n$ denotes the control input at the joint/thruster level, $\boldsymbol{M}(\boldsymbol{q})$ is the positive definite inertial matrix, $\boldsymbol{C}(\boldsymbol{q},\boldsymbol{\zeta})$ represents coriolis and centrifugal terms, $\boldsymbol{D}(\boldsymbol{q},\boldsymbol{\zeta})$ models damping effects, and $\boldsymbol{g}(\boldsymbol{q})$ encapsulates the gravity and buoyancy effects.

B. IBVS Modeling

Next, we will explain the IBVS model. The camera frame $\{\mathcal{C}\}$, which is rigidly attached to the center of the camera O_c, has its axes represented by $[X_c, Y_c, Z_c]^\top$. The image frame $\{\mathcal{I}_m\}$ is represented by the coordinates $[u, v]^\top$, with its center being O_{im} (see Fig. 2). The camera geometrical

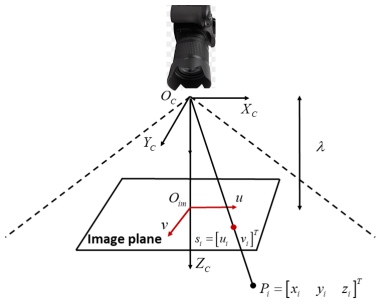

Fig. 2. Modeling of a central projection camera sensor.

model involves projecting a collection of n three-dimensional points, denoted as $\mathbf{p_i} = [x_i, y_i, z_i]^T$ for $i = 1, \ldots, n$, which are expressed in the camera frame, onto the corresponding two-dimensional image features, denoted as $\boldsymbol{s_i} = [u_i, v_i]^T$ for $i = 1, \ldots, n$, in pixels. This process is described as follows [23]:

$$\boldsymbol{s_i} = \begin{bmatrix} u_i \\ v_i \end{bmatrix} = \frac{\lambda}{z_i}\begin{bmatrix} x_i \\ y_i \end{bmatrix} \tag{3}$$

where λ represents the focal length of the camera. The time derivative of the image features can be linked to the velocity of the camera as:

$$\dot{\boldsymbol{s}}_{\boldsymbol{i}} = \boldsymbol{L}_i(z_i, s_i)\boldsymbol{v_c},\ i = 1, \ldots, n \tag{4}$$

where:

$$\boldsymbol{L}_i(z_i,s_i) = \begin{bmatrix} -\frac{\lambda}{z_i} & 0 & \frac{u_i}{z_i} & \frac{u_iv_i}{\lambda} & -\frac{\lambda^2+u_i^2}{\lambda} & v_i \\ 0 & -\frac{\lambda}{z_i} & \frac{v_i}{z_i} & \frac{\lambda^2+v_i^2}{\lambda} & -\frac{u_iv_i}{\lambda} & -u_i \end{bmatrix} \tag{5}$$

is the interaction matrix [24], and $\boldsymbol{v}_c \triangleq \begin{bmatrix} \boldsymbol{t}_c^T,\ \boldsymbol{\omega}_c^T \end{bmatrix}^T$ denotes the linear $\boldsymbol{t}_c$ and angular $\boldsymbol{\omega}_c$ velocities of the camera frame. Let $\boldsymbol{s} = \begin{bmatrix} s_1^T, \cdots, s_n^T \end{bmatrix}^T \in \Re^{2n}$ be the overall image feature vector. Hence, the time-derivative of the image features is given by:

$$\dot{\boldsymbol{s}} = \boldsymbol{L}(z, s)\boldsymbol{v_c} \tag{6}$$

where $\boldsymbol{L}(z,s) = \left[\boldsymbol{L}_1^T(z_1,s_1), \cdots, \boldsymbol{L}_n^T(z_n,s_n)\right]^T \in \Re^{2n\times 6}$ is the overall interaction matrix and $\boldsymbol{z} = [z_1,\ldots,z_n]^T$. The restricted camera FoV, imposes the following visibility constraints:

$$u_{\min} \leq u_i \leq u_{\max},\ i = 1,\ldots,n \tag{7a}$$
$$v_{\min} \leq v_i \leq v_{\max},\ i = 1,\ldots,n \tag{7b}$$

where $u_{\min}$, $v_{\min}$ and $u_{\max}$, $v_{\max}$ represent the image plane coordinates' lower and upper bounds (in pixels), according to the camera resolution.

III. Control Methodology

The proposed CBF visual servoing control scheme has two parts: i) a CBF-IBVS controller calculating velocity commands at the UVMS camera frame while respecting FoV constraints, and ii) a CBF velocity controller for the overall UVMS, tracking CBF-IBVS commands while adhering to system velocity limits.

A. CBF-IBVS Control design

Considering the dynamical system described in Eq. 6 and defining the image errors as following:

$$e_{u_i}(t) = u_i(t) - u_{d_i},\ i = 1,\ldots,n \tag{8a}$$
$$e_{v_i}(t) = v_i(t) - v_{d_i},\ i = 1,\ldots,n \tag{8b}$$

where u_{d_i}, v_{d_i} are the desired image features and $\boldsymbol{e} \triangleq [e_{u_1}, e_{v_1}, \ldots, e_{u_n}, e_{v_n}]^T$ is the overall error, we are able to formulate the following nominal control law [24] for the velocity of the camera frame:

$$\boldsymbol{v}_c(\boldsymbol{z},\boldsymbol{s},t) = -\gamma \boldsymbol{L}^{\dagger}(\boldsymbol{z},\boldsymbol{s},t)\boldsymbol{e} \tag{9}$$

Next, we proceed with the incorporation of the FoV constraints, defined in Eq. 7, by employing the CBF notion. Following the results given in [25], we consider the logarithmic Barrier Functions of the form:

$$B_u(u_i, \underline{M}_{u_i}, \overline{M}_{u_i}) = \ln\left(\frac{\overline{M}_{u_i}}{\underline{M}_{u_i}}\frac{\underline{M}_{u_i} - u_i}{\overline{M}_{u_i} - u_i}\right) \tag{10a}$$
$$B_v(v_i, \underline{M}_{v_i}, \overline{M}_{v_i}) = \ln\left(\frac{\overline{M}_{v_i}}{\underline{M}_{v_i}}\frac{\underline{M}_{v_i} - v_i}{\overline{M}_{v_i} - v_i}\right) \tag{10b}$$

$\forall u_i \in (\underline{M}_{u_i}, \overline{M}_{u_i})$, $\forall v_i \in (\underline{M}_{v_i}, \overline{M}_{v_i})$ where $\underline{M}_{u_i} = \frac{u_{min}-c_u}{a_u}$, $\underline{M}_{v_i} = \frac{v_{min}-c_v}{a_v}$, $\overline{M}_{u_i} = \frac{u_{max}-c_u}{a_u}$, $\overline{M}_{v_i} = \frac{v_{max}-c_v}{a_v}$, c_u, c_v the image center coordinates and a_u, a_v the camera focal lengths in pixels.

Then we define the following transformed constrained states $\boldsymbol{\xi}_{s_i} = [\xi_{u_i}, \xi_{v_i}]^T$, where:

$$\xi_{u_i} = B_u(u_i, \underline{M}_{u_i}, \overline{M}_{u_i}) \tag{11a}$$
$$\xi_{v_i} = B_v(v_i, \underline{M}_{v_i}, \overline{M}_{v_i}) \tag{11b}$$

and due to monotonic property of the natural logarithm, it holds:

$$u_i = B_u^{-1}(\xi_{u_i}, \underline{M}_{u_i}, \overline{M}_{u_i}) \tag{12a}$$
$$v_i = B_v^{-1}(\xi_{v_i}, \underline{M}_{v_i}, \overline{M}_{v_i}) \tag{12b}$$

and in analytical form:

$$u_i = \frac{\underline{M}_{u_i}\overline{M}_{u_i}\left(-e^{-\frac{\xi_{u_i}}{2}} + e^{\frac{\xi_{u_i}}{2}}\right)}{-\overline{M}_{u_i}e^{-\frac{\xi_{u_i}}{2}} + \underline{M}_{u_i}e^{\frac{\xi_{u_i}}{2}}} \tag{13a}$$
$$v_i = \frac{\underline{M}_{v_i}\overline{M}_{v_i}\left(-e^{-\frac{\xi_{v_i}}{2}} + e^{\frac{\xi_{v_i}}{2}}\right)}{-\overline{M}_{v_i}e^{-\frac{\xi_{v_i}}{2}} + \underline{M}_{v_i}e^{\frac{\xi_{v_i}}{2}}} \tag{13b}$$

Differentiating Eq. 13a, 13b, yields:

$$\frac{\partial u_i}{\partial \xi_{u_i}} = \frac{\overline{M}_{u_i}\underline{M}_{u_i}^2 - \underline{M}_{u_i}\overline{M}_{u_i}^2}{\underline{M}_{u_i}^2 e^{\xi_{u_i}} - 2\underline{M}_{u_i}\overline{M}_{u_i} + \overline{M}_{u_i}^2 e^{-\xi_{u_i}}} \tag{14a}$$
$$\frac{\partial v_i}{\partial \xi_{v_i}} = \frac{\overline{M}_{v_i}\underline{M}_{v_i}^2 - \underline{M}_{v_i}\overline{M}_{v_i}^2}{\underline{M}_{v_i}^2 e^{\xi_{v_i}} - 2\underline{M}_{v_i}\overline{M}_{v_i} + \overline{M}_{v_i}^2 e^{-\xi_{v_i}}} \tag{14b}$$

The transformed dynamical system takes the following form:

$$\dot{\boldsymbol{\xi}}_{s_i} = \boldsymbol{K_i}\boldsymbol{L}(z,s_i,t)\boldsymbol{v_c} \tag{15}$$

where $\boldsymbol{K_i} \in \Re^{2x2}$ and $\boldsymbol{K_i} = \begin{bmatrix} \left(\frac{\partial u_i}{\partial \xi_{u_i}}\right)^{-1} & 0 \\ 0 & \left(\frac{\partial v_i}{\partial \xi_{v_i}}\right)^{-1} \end{bmatrix}$.

Hence, the control law:

$$\boldsymbol{v}_c^r(\boldsymbol{z},\boldsymbol{s},t) = -\gamma \boldsymbol{L}^{\dagger}(\boldsymbol{z},\boldsymbol{s},t)\boldsymbol{K}^T\boldsymbol{e}_{\xi} \tag{16}$$

where $\boldsymbol{e}_{\xi} = [\boldsymbol{e}_{\xi_1}\ldots\boldsymbol{e}_{\xi_n}]$, $\boldsymbol{e}_{\xi_i} = \left[e_{\xi_{u_i}}, e_{\xi_{v_i}}\right]$, $e_{\xi_{u_i}} = \xi_{u_i} - \xi_{u_{i_d}}$, $e_{\xi_{v_i}} = \xi_{v_i} - \xi_{v_{i_d}}$, guarantees local asymptotic stability to the desired configuration, while simultaneously satisfying FoV constraints.

B. Handling of Operational Limitations

The camera's frame, denoted as $\{\mathcal{C}\}$, which is firmly attached at the End-Effector's origin O_C, does not align with the End-Effector frame $\{E\}$. Hence, by utilizing a spatial motion transformation matrix ${}^e\boldsymbol{V}_c \in \Re^{6\times 6}$, the CBF-IBVS described in equation (17) can be transformed from the camera frame to the End-Effector frame [26]:

$$\boldsymbol{v}_e^r(\boldsymbol{z},\boldsymbol{s},t) = {}^e\boldsymbol{V}_c\ \boldsymbol{v}_c^r(\boldsymbol{z},\boldsymbol{s},t) \tag{17}$$

The desired End-Effector motion profile $\boldsymbol{v}_e^r(s,t)$ is transformed to the configuration space as in [27]:

$$\boldsymbol{\zeta}^r(t) = \boldsymbol{J}(\boldsymbol{q})^{\#}\boldsymbol{v}_e^r + \left(\boldsymbol{I}_{n\times n} - \boldsymbol{J}(\boldsymbol{q})^{\#}\boldsymbol{J}(\boldsymbol{q})\right)\boldsymbol{v}_e^0 \in \Re^n \tag{18}$$

where $\boldsymbol{J}(\boldsymbol{q})^{\#}$ is the generalized pseudo-inverse of the Jacobian, and $\boldsymbol{v}_e^0$ represents secondary tasks [28] to be tuned independently to satisfy operational limitations like manipulator's joint limits since they don't affect the end-effector's velocity [29]. The proposed scheme enables desired image feature tracking alongside visibility constraint satisfaction. Therefore, these can be equally prioritized as primary tasks and treat various other operational limitations (e.g., joint limits) as secondary tasks in a fully decoupled manner. More details on task priority based control can be found in [29], [30].

C. Control Barrier Function Based Velocity Control

Given the desired configuration space motion profile $\boldsymbol{\zeta}^r(t)$ in (18) that satisfies different operational limitations, we proceed with the design of a velocity controller based on Zeroing CBF, that achieves certain predefined minimum speed of response.

Definition 1: [15] Zeroing Control Barrier Functions: Consider the system

$$\dot{x} = f(x) + g(x)u \tag{19}$$

, where $f(\cdot)$ and $g(\cdot)$ are locally Lipschitz functions and u is constrained in a compact set $U \subset \mathbb{R}^m$. Let $\mathcal{C}_b \subset D$ be the superlevel set of a continuously differentiable function $b : D \subset \mathbb{R}^n \to \mathbb{R}$, i.e., $\mathcal{C}_b := \{x \in \mathbb{R}^n : b(x) \geq 0\}$. Then, b is a zeroing control barrier function (ZCBF) for the system (19) if there exists an extended class $\mathcal{K}_\infty$ function α such that

$$\sup_{u \in U} [\nabla b(x)^\top (f(x) + g(x)u) + \alpha(b(x))] \geq 0, x \in D. \tag{20}$$

Similar to the CBF-IBVS, the first step is to define the velocity error vector:

$$\boldsymbol{e}_\zeta(t) \triangleq [e_{\zeta_1}(t), \ldots, e_{\zeta_n}(t)]^\top = \boldsymbol{\zeta}(t) - \boldsymbol{\zeta}^r(t) \in \Re^n \tag{21}$$

Notice that similarly to the image features' errors we aim to impose bounded response on the system velocities errors $e_{\zeta_i}(t), i = 1, \ldots, n$ as well by satisfying:

$$-\rho_{\zeta_i} < e_{\zeta_i}(t) < \rho_{\zeta_i}, \ \forall t \geq 0 \ i = 1, \ldots, n \tag{22}$$

where, $\rho_{\zeta_i}, i = 1, \ldots, n$ is the predefined velocity bound that is set according to each system DoF. We define the new error vector

$$\xi = \xi(\boldsymbol{\zeta}, t) := \rho_\zeta^{-1} e_\zeta(t) \tag{23}$$

where $\rho_\zeta := \text{diag}(\rho_{\zeta_i})$, $i = 1, \ldots, n$. The control objective is then equivalent to maintaining the normalized error $\xi(t)$ in the set $(-1, 1)$. For this aim, we define the continuously differentiable barrier function $b : \mathbb{R}^n \times \mathbb{R}_{\geq 0} \to \mathbb{R}$ and its 0-superlevel set as

$$b(\boldsymbol{\zeta}, t) := \frac{1}{2}(1 - \|\xi\|^2) = \frac{1}{2}(1 - \|\xi(\boldsymbol{\zeta}, t)\|^2),$$
$$\mathcal{C}_b(t) := \{\boldsymbol{\zeta} \in \mathbb{R}^n : \frac{1}{2}(1 - d^2) \geq b(\boldsymbol{\zeta}, t) \geq 0\}.$$

where the constant $0 < d < 1$ with $d \leq \|\xi\|$ is considered for the sake of controllability maintenance. The goal is to render the set $\mathcal{C}_b(t)$ forward invariant, i.e., to guarantee that $\boldsymbol{\zeta}(t) \in \mathcal{C}_b(t), \forall t \geq 0$, provided that $\boldsymbol{\zeta}(0) \in \mathcal{C}_b(0)$ [15]. By evaluating the derivative of $b(\boldsymbol{\zeta}, t)$ along the system dynamics (2), one obtains

$$\frac{\partial b(\boldsymbol{\zeta}, t)}{\partial \boldsymbol{\zeta}} \dot{\zeta} + \frac{\partial b(\boldsymbol{\zeta}, t)}{\partial t} = -\xi^\top \rho^{-1} (\boldsymbol{\zeta} - \boldsymbol{\zeta}^r) \dot{\xi}$$
$$= -\xi^\top \rho^{-1} (\boldsymbol{\zeta} - \boldsymbol{\zeta}^r) \boldsymbol{M}^{-1}(\boldsymbol{q})$$
$$\times (-\boldsymbol{C}(\boldsymbol{q}, \boldsymbol{\zeta})\boldsymbol{\zeta} - \boldsymbol{D}(\boldsymbol{q}, \boldsymbol{\zeta})\boldsymbol{\zeta} - \boldsymbol{g}(\boldsymbol{q}) - \boldsymbol{\delta}(\boldsymbol{q}, \boldsymbol{\zeta}, t) + \boldsymbol{\tau}).$$

Consider the set

$$K(\boldsymbol{\zeta}, \boldsymbol{q}, t) = \{\boldsymbol{\tau} \in \Re^n : -\xi^\top \rho^{-1} (\boldsymbol{\zeta} - \boldsymbol{\zeta}^r) \boldsymbol{M}^{-1}(\boldsymbol{q})$$
$$\times (-\boldsymbol{C}(\boldsymbol{q}, \boldsymbol{\zeta})\boldsymbol{\zeta} - \boldsymbol{D}(\boldsymbol{q}, \boldsymbol{\zeta})\boldsymbol{\zeta} - \boldsymbol{g}(\boldsymbol{q}) - \boldsymbol{\delta}(\boldsymbol{q}, \boldsymbol{\zeta}, t) + \boldsymbol{\tau})$$
$$+ \alpha(\frac{1}{2}(1 - \|\xi\|^2)) \geq 0\}. \tag{24}$$

According to Definition 1, if there exists an extended class $\mathcal{K}_\infty$ function α such that the set $K(\boldsymbol{\zeta}, \boldsymbol{q}, t)$ is non-empty for all $\boldsymbol{\zeta}$, the function $b(\boldsymbol{\zeta}, t)$ is a ZCBF. However, $\delta(\boldsymbol{q}, \boldsymbol{\zeta}, t)$ is an unknown disturbance term and we can not use it in the definition of the set $K(\boldsymbol{\zeta}, \boldsymbol{q}, t)$. As we assume the upper bound of this term is known as $\bar{\delta} \geq \delta(\boldsymbol{q}, \boldsymbol{\zeta}, t) > 0, \forall (\boldsymbol{q}, \boldsymbol{\zeta}, t)$, we can define a more conservative set $\bar{K}(\boldsymbol{\zeta}, \boldsymbol{q}, t)$ that also represents a subset of the set $K(\boldsymbol{\zeta}, \boldsymbol{q}, t)$ in (24) as below

$$\bar{K}(\boldsymbol{\zeta}, \boldsymbol{q}, t) = \{\boldsymbol{\tau} \in \Re^n : -\xi^\top \rho^{-1} (\boldsymbol{\zeta} - \boldsymbol{\zeta}^r) \boldsymbol{M}^{-1}(\boldsymbol{q})$$
$$\times (-\boldsymbol{C}(\boldsymbol{q}, \boldsymbol{\zeta})\boldsymbol{\zeta} - \boldsymbol{D}(\boldsymbol{q}, \boldsymbol{\zeta})\boldsymbol{\zeta} - \boldsymbol{g}(\boldsymbol{q}) + \boldsymbol{\tau})$$
$$+ \alpha(\frac{1}{2}(1 - \|\xi\|^2)) - \bar{\delta}\|\xi^\top \rho^{-1} (\boldsymbol{\zeta} - \boldsymbol{\zeta}^r) \boldsymbol{M}^{-1}(\boldsymbol{q})\| \geq 0\}. \tag{25}$$

The non-emptiness of $\bar{K}(\boldsymbol{\zeta}, \boldsymbol{q}, t)$ implicates the standard ZCBF-based conditions, such as (20) and the ones in [15]. The control design consists of computing a controller that satisfies $\boldsymbol{\tau}(\boldsymbol{\zeta}, \boldsymbol{q}, t) \in \bar{K}(\boldsymbol{\zeta}, \boldsymbol{q}, t)$ for all $(\boldsymbol{\zeta}, \boldsymbol{q}, t)$, given a ZCBF function $b(\boldsymbol{\zeta}, t)$.

Accordingly, we consider the quadratic program

$$\tau^*(\boldsymbol{\zeta}, \boldsymbol{q}, t) = argmin_{\boldsymbol{\tau} \in \Re^n} \|\tau\|^2 \tag{26}$$

s.t

$$-\xi^\top \rho^{-1} (\boldsymbol{\zeta} - \boldsymbol{\zeta}^r) \boldsymbol{M}^{-1}(\boldsymbol{q}) (-\boldsymbol{C}(\boldsymbol{q}, \boldsymbol{\zeta})\boldsymbol{\zeta} - \boldsymbol{D}(\boldsymbol{q}, \boldsymbol{\zeta})\boldsymbol{\zeta} - \boldsymbol{g}(\boldsymbol{q})$$
$$+ \boldsymbol{\tau}) + \alpha(\frac{1}{2}(1 - \|\xi\|^2)) - \bar{\delta}\|\xi^\top \rho^{-1} (\boldsymbol{\zeta} - \boldsymbol{\zeta}^r) \boldsymbol{M}^{-1}(\boldsymbol{q})\| \geq 0.$$

Given a function $b(\boldsymbol{\zeta}, t)$, the feasibility of (26) for $(\boldsymbol{\zeta}, \boldsymbol{q}, t)$ guarantees that $b(\boldsymbol{\zeta}, t)$ is a ZCBF.

IV. Simulation Results

A. System Components and Parameters

We performed a realistic simulation using the UwSim dynamic simulator [31] on the Robot Operating System (ROS) [32] to verify the proposed CBF-IBVS approach for Underwater Vehicle Manipulator Systems. The UVMS includes a 4 DoFs underwater vehicle and a 4 DoF manipulator where a camera with resolution 640×480 pixels is attached at its end-effector. A visual target of four markers is placed within the workspace, each marker detected as an image feature using the Computer Vision ArToolkit library [33]. The UVMS initialized in a configuration where the target is visible (see Fig.3). The proposed CBF-IBVS scheme is tested in a scenario with a fixed target, aiming to stabilize the camera to a predefined configuration.

The simulation aim is to drive the feature vector $\boldsymbol{s}$ to the desired configuration $\boldsymbol{s}_d$ inside the image plane using the proposed CBF-IBVS control scheme, as shown in Fig.3. This initial pose is challenging for IBVS schemes due to significant camera rotation around the x-axis and

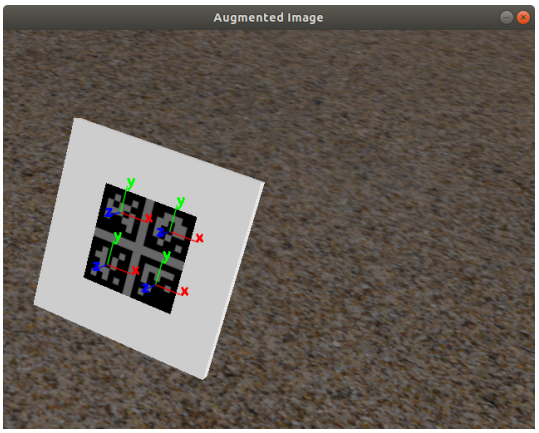

(a) Initial pose configuration

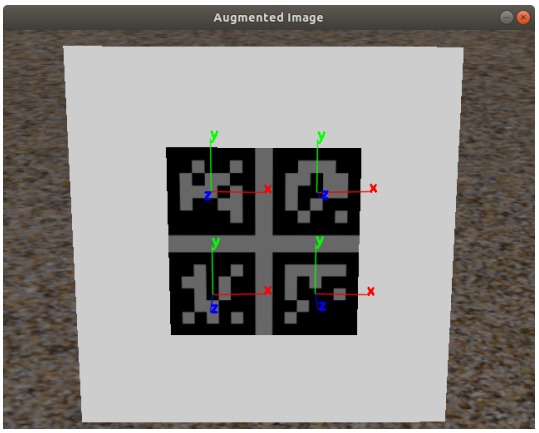

(b) Desired pose configuration

Fig. 3. Experimental setup: a) Initial pose configuration, b) desired pose configuration. The initial configuration is rather challenging for IBVS schemes, owing to the large rotation of the camera frame as well as the large distance relative to the target configuration. The proposed CBF-IBVS control scheme successfully guides the UVMS to the desired configuration while simultaneously satisfying all the operational limitations.

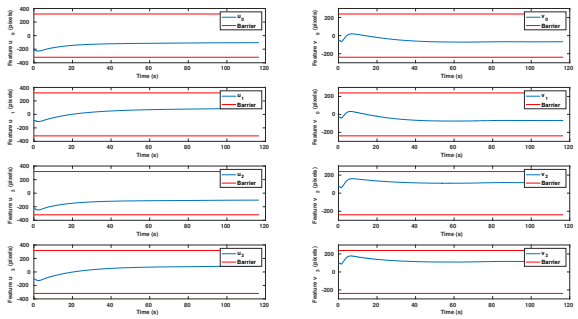

Fig. 4. Simulation Study I: The evolution of the feature coordinates along with the corresponding imposed bounds.

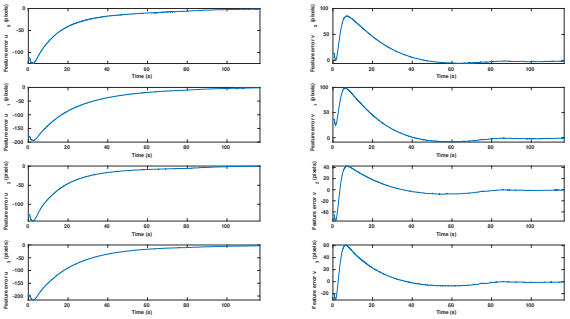

Fig. 5. Simulation Study I: The evolution of the feature coordinate errors.

the target's distance. Desired feature coordinates $s_d = \begin{bmatrix} 251 & 379 & 251 & 379 \\ 196 & 196 & 318 & 318 \end{bmatrix}$ were extracted from a still image at the camera's desired pose. The controller is designed to maintain object visibility within the camera's field of view and respect operational limitations like vehicle and manipulator joint velocity limits. The visibility constraints were set as $u_{min} = -319$, $u_{max} = 319$, $v_{min} = -239$, $v_{max} = 239$, and used to define the barriers $\underline{M}_{u_i}, \overline{M}_{u_i}$, $\underline{M}_{u_i}, \overline{M}_{u_i}$ for $i = 1 \dots 4$. The velocity limits were set to $[-0.5, 0.5]$ for the vehicle Dofs and $[-0.1, 0.1]$ for manipulator joints. The results are indicated in Figs. 4-7. The evolution of image features is depicted in n Fig. 4, showing that the FoV constraints where satisfied at all times. Fig.4 shows FoV constraints were satisfied, and Fig.5 demonstrates smooth convergence of feature errors to zero. Moreover, system velocity errors remained within bounds (Figs.6, 7), and desired system velocities were effectively tracked.

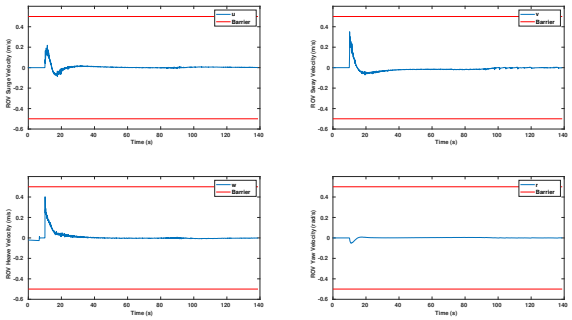

Fig. 6. Simulation Study I: The evolution of the vehicle (ROV) velocities along with their corresponding bounds.

V. Conclusions

This paper introduced a novel control strategy for underwater vehicle manipulator systems, integrating control barrier functions with image-based visual servoing to address operational limitations, visibility constraints, and system uncertainties. The proposed control methodology is structured in two stages where in the first stage, a CBF-IBVS controller calculates the commands at the UVMS camera frame, ensuring field-of-view compliance, while at the second stage, a CBF velocity controller tracks these commands, while respecting system velocity limits. The simulation results validated the effectiveness of the proposed approach, showing improved performance, safety, and robustness compared to traditional IBVS methods, and with low complexity that

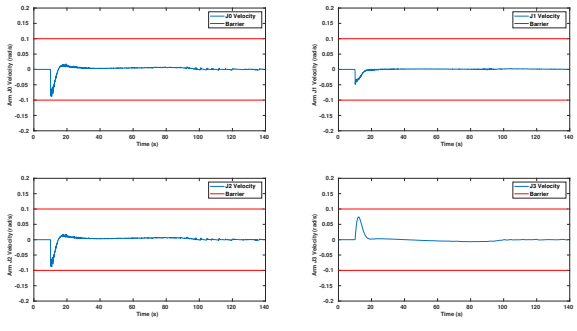

Fig. 7. Simulation Study I: The evolution of the manipulator joint velocities along with their corresponding bounds.

makes it easy to implement in embedded on-board computer systems. Further studies may be necessary to validate the proposed approach in real-world applications and explore its potential for other types of robotic systems.

REFERENCES

[1] S. Heshmati-Alamdari, G. C. Karras, P. Marantos, and K. J. Kyriakopoulos, "A robust model predictive control approach for autonomous underwater vehicles operating in a constrained workspace," in *2018 IEEE International Conference on Robotics and Automation (ICRA)*, pp. 6183–6188, IEEE, 2018.

[2] P. Ridao, M. Carreras, D. Ribas, P. Sanz, and G. Oliver, "Intervention auvs: The next challenge," *Annual Reviews in Control*, vol. 40, pp. 227–241, 2015.

[3] H. Farivarnejad and S. Moosavian, "Multiple impedance control for object manipulation by a dual arm underwater vehicle-manipulator system," *Ocean Engineering*, vol. 89, pp. 82–98, 2014.

[4] G. C. Karras, G. K. Fourlas, A. Nikou, C. P. Bechlioulis, and S. Heshmati-Alamdari, "Image based visual servoing for floating base mobile manipulator systems with prescribed performance under operational constraints," *Machines*, vol. 10, no. 7, p. 547, 2022.

[5] S. Heshmati-Alamdari, G. C. Karras, and K. J. Kyriakopoulos, "A distributed predictive control approach for cooperative manipulation of multiple underwater vehicle manipulator systems," in *2019 international conference on robotics and automation (ICRA)*, pp. 4626–4632, IEEE, 2019.

[6] P. Londhe, S. Mohan, B. Patre, and L. Waghmare, "Robust task-space control of an autonomous underwater vehicle-manipulator system by pid-like fuzzy control scheme with disturbance estimator," *Ocean Engineering*, vol. 139, pp. 1–13, 2017.

[7] H. Lang, M. T. Khan, K.-K. Tan, and C. W. de Silva, "Developments in visual servoing for mobile manipulation," *Unmanned Systems*, vol. 1, no. 01, pp. 143–162, 2013.

[8] S. Heshmati-Alamdari, A. Eqtami, G. C. Karras, D. V. Dimarogonas, and K. J. Kyriakopoulos, "A self-triggered position based visual servoing model predictive control scheme for underwater robotic vehicles," *Machines*, vol. 8, no. 2, p. 33, 2020.

[9] D. Chrysostomou, A. Gasteratos, L. Nalpantidis, and G. C. Sirakoulis, "Multi-view 3d scene reconstruction using ant colony optimization techniques," *Measurement Science and Technology*, vol. 23, no. 11, p. 114002, 2012.

[10] F. Chaumette and S. Hutchinson, "Visual servo control. i. basic approaches," *IEEE Robotics and Automation Magazine*, vol. 13, no. 4, pp. 82–90, 2006.

[11] F. Chaumette and S. Hutchinson, "Visual servo control, part ii: Advanced approaches," *IEEE Robotics and Automation Magazine*, vol. 14, no. 1, pp. 109–118, 2007.

[12] G. C. Karras, C. P. Bechlioulis, G. K. Fourlas, and K. J. Kyriakopoulos, "Target tracking with multi-rotor aerial vehicles based on a robust visual servo controller with prescribed performance," in *2020 International Conference on Unmanned Aircraft Systems (ICUAS)*, pp. 480–487, IEEE, 2020.

[13] S. Heshmati-alamdari, C. P. Bechlioulis, M. V. Liarokapis, and K. J. Kyriakopoulos, "Prescribed performance image based visual servoing under field of view constraints," in *IEEE/RSJ International Conference on Intelligent Robots and Systems (IROS)*, September 2014.

[14] S. Heshmati-Alamdari, G. C. Karras, and K. J. Kyriakopoulos, "A predictive control approach for cooperative transportation by multiple underwater vehicle manipulator systems," *IEEE Transactions on Control Systems Technology*, 2021.

[15] A. D. Ames, X. Xu, J. W. Grizzle, and P. Tabuada, "Control barrier function based quadratic programs for safety critical systems," *IEEE Transactions on Automatic Control*, vol. 62, no. 8, pp. 3861–3876, 2016.

[16] J. F. Fisac, A. K. Akametalu, M. N. Zeilinger, S. Kaynama, J. Gillula, and C. J. Tomlin, "A general safety framework for learning-based control in uncertain robotic systems," *IEEE Transactions on Automatic Control*, vol. 64, no. 7, pp. 2737–2752, 2018.

[17] L. Wang, E. A. Theodorou, and M. Egerstedt, "Safe learning of quadrotor dynamics using barrier certificates," in *2018 IEEE International Conference on Robotics and Automation (ICRA)*, pp. 2460–2465, IEEE, 2018.

[18] S. Wu, T. Liu, Q. Niu, and Z.-P. Jiang, "Continuous safety control of mobile robots in cluttered environments," *IEEE Robotics and Automation Letters*, vol. 7, no. 3, pp. 8012–8019, 2022.

[19] E. H. Thyri, E. A. Basso, M. Breivik, K. Y. Pettersen, R. Skjetne, and A. M. Lekkas, "Reactive collision avoidance for asvs based on control barrier functions," in *2020 IEEE Conference on Control Technology and Applications (CCTA)*, pp. 380–387, IEEE, 2020.

[20] M. Sharifi and D. V. Dimarogonas, "Higher order barrier certificates for leader-follower multi-agent systems," *IEEE Trans. Control Network Syst.*, 2022.

[21] G. P. Kontoudis and K. G. Vamvoudakis, "Kinodynamic motion planning with continuous-time q-learning: An online, model-free, and safe navigation framework," *IEEE transactions on neural networks and learning systems*, vol. 30, no. 12, pp. 3803–3817, 2019.

[22] G. Antonelli, *"Underwater Robots"*. Springer Tracts in Advanced Robotics, Springer International Publishing, 2013.

[23] S. Heshmati-Alamdari, G. C. Karras, A. Eqtami, and K. J. Kyriakopoulos, "A robust self triggered image based visual servoing model predictive control scheme for small autonomous robots," in *2015 IEEE/RSJ International Conference on Intelligent Robots and Systems (IROS)*, pp. 5492–5497, IEEE, 2015.

[24] G. H. S. Hutchinson and P. Corke, "A tutorial on visual servo control," *IEEE Transactions on Robotics and Automation*, vol. 12, no. 6, pp. 651–670, 1996.

[25] I. Salehi, G. Rotithor, R. Saltus, and A. P. Dani, "Constrained image-based visual servoing using barrier functions," in *2021 IEEE International Conference on Robotics and Automation (ICRA)*, pp. 14254–14260, 2021.

[26] F. Chaumette and S. Hutchinson, "Visual servo control. ii. advanced approaches [tutorial]," *IEEE Robotics and Automation Magazine*, vol. 14, no. 1, pp. 109–118, 2007.

[27] S. Heshmati-alamdari, A. Nikou, K. J. Kyriakopoulos, and D. V. Dimarogonas, "A robust force control approach for underwater vehicle manipulator systems," *IFAC-PapersOnLine*, vol. 50, no. 1, pp. 11197–11202, 2017.

[28] B. Siciliano and J. J. E. Slotine, "A general framework for managing multiple tasks in highly redundant robotic systems," *Advanced Robotics, 1991. 'Robots in Unstructured Environments', 91 ICAR., Fifth International Conference on*, pp. 1211–1216 vol.2, 1991.

[29] E. Simetti and G. Casalino, "A novel practical technique to integrate inequality control objectives and task transitions in priority based control," *Journal of Intelligent and Robotic Systems: Theory and Applications*, vol. 84, no. 1-4, pp. 877–902, 2016.

[30] S. Soylu, B. Buckham, and R. Podhorodeski, "Redundancy resolution for underwater mobile manipulators," *Ocean Engineering*, vol. 37, no. 2-3, pp. 325–343, 2010.

[31] M. Prats, J. Perez, J. Fernandez, and P. Sanz, "An open source tool for simulation and supervision of underwater intervention missions," in *IEEE/RSJ International Conference on Intelligent Robots and Systems (IROS)*, pp. 2577–2582, 2012.

[32] M. Quigley, K. Conley, B. P. Gerkey, J. Faust, T. Foote, J. Leibs, R. Wheeler, and A. Y. Ng, "Ros: an open-source robot operating system," *ICRA Workshop on Open Source Software*, 2009.

[33] H. Kato and M. Billinghurst, "Marker tracking and hmd calibration for a video-based augmented reality conferencing system," *Proceedings of the 2nd International Workshop on Augmented Reality (IWAR 99)*, 1999.